Quadrature Element Vibration Analysis of Arbitrarily Shaped Membranes

WANG Xinwei[1*], *CAI Deng'an*, *ZHOU Guangming*

State Key Laboratory of Mechanics and Control of Mechanical Structures, Nanjing University of Aeronautics and Astronautics, Nanjing 210016, P.R. China

(Received 8 March 2021; revised 23 May 2021; accepted 20 December 2021)

Abstract: The aim of the present study is to develop an efficient weak form quadrature element for free vibration analysis of arbitrarily shaped membranes. The arbitrarily shaped membrane is firstly mapped into a regular domain using blending functions, and the displacement in the element is assumed as the trigonometric functions. Explicit formulations are worked out for nodes of any type and a varying number of nodes. For verifications, results are compared with exact solutions and data obtained by other numerical methods. It is demonstrated that highly accurate frequencies can be obtained with a small number of nodes by present method.

Key words: arbitrarily shaped membrane; free vibration; quadrature element; blending function

CLC number: V214 **Document code:** A **Article ID:** 1005-1120(2022)01-0001-11

0 Introduction

A membrane is characterized by a negligible resistance to bending and a dominating tension. Numerous membrane structures exist in practice and their applications are still growing in importance[1]. Therefore, free vibration of membranes has attracted the attention of many researchers[2-7]. A review on the study of the membrane vibration was given by Jenkins and Korde recently[1].

Numerical modeling and analysis of structural elements with irregular shapes have continuously been a popular research topic because of the widespread applications of irregular shaped elements in various fields[8]. Besides, the enhancement of computational efficiency and accuracy has always been an interesting research topic to the computational mechanics community[9]. Several efficient numerical methods, such as the strong form differential quadrature element method (DQEM)[10], the local radial basis function-based differential quadrature (LRBFDQ)[7], the discrete singular convolution (DSC) algorithm[11] and the weak form quadrature element method (QEM)[12], have been developed recently and are still under developing, since an efficient numerical method is always valuable to designers in certain engineering applications[13].

Free vibration of membranes is the simplest two-dimensional vibration problem and thus it is often used to test the performance of a numerical technique, e.g., the collocation method[2], the p-version finite element method (p-FEM)[3], the DSC algorithm[4], the DQEM[5-6], and LRBFDQ[7]. For arbitrary shaped membranes, the irregular domain is usually mapped into a regular domain by using either blending functions[3,6], or shape functions of a Serendipity element[4-5]. Care should be taken that, however, the mapping accuracy affects the solution accuracy[5-6,14] and that inaccurate mapping may even

*Corresponding author, E-mail address: wangx@nuaa.edu.cn.

How to cite this article: WANG Xinwei, CAI Deng'an, ZHOU Guangming. Quadrature element vibration analysis of arbitrarily shaped membranes[J]. Transactions of Nanjing University of Aeronautics and Astronautics, 2022, 39(1): 1-11.

http://dx.doi.org/10.16356/j.1005-1120.2022.01.001

cause non-convergent results if the irregular shape does not have four corners[15-16], since zero or negative Jacobian determinant will inevitably occur at the corners[16]. Numerical difficulty may be encountered since the derivative with respect to x and/or y at the corner points does not exist. In such cases, the weak form methods may have some advantages over the strong form methods, since the numerical difficulty may be circumvented using Gauss quadrature[16].

Previous research showed that the QEM was highly accurate[9,12,17-19] and possessed the potential to act as a competitive counterpart to other efficient numerical methods and thus was worth being developed further[9]. An undisputable advantage of the QEM over the p-FEM is that the pre- and post-processing is much more convenient due to the physical meaning of its DOFs[19]. Therefore, the objective of present paper is to develop an efficient quadrature element for the free vibration analysis of arbitrarily shaped membranes. The arbitrarily shape is firstly mapped into a regular domain using blending functions and the discretization is then done on the regular domain. Trigonometric functions are used as the element displacement to formulate a sub-parametric element. Explicit formulations are given for the element with nodes of any type and a varying number of nodes. Numerical examples are given. The obtained results are compared with exact solutions and data obtained by other numerical methods for verifications. Finally conclusions are drawn.

1 Weak Form Quadrature Element Formulations

1.1 Expressions of potential energy and kinetic energy

For the investigation of the free vibration behavior of membranes by a weak form method, the expressions of potential energy U and kinetic energy T of the element are needed and given as

$$U=\frac{S}{2}\iint_A\left[\left(\frac{\partial w}{\partial x}\right)^2+\left(\frac{\partial w}{\partial y}\right)^2\right]\mathrm{d}A=$$
$$\frac{1}{2}\int_{-1}^{1}\int_{-1}^{1}\left[\left(\frac{\partial w}{\partial x}\right)^2+\left(\frac{\partial w}{\partial y}\right)^2\right]|\boldsymbol{J}|\,\mathrm{d}\xi\mathrm{d}\eta \tag{1}$$

$$T=\frac{1}{2}\iint_A\rho\dot{w}^2\mathrm{d}A=\frac{1}{2}\int_{-1}^{1}\int_{-1}^{1}\rho\dot{w}^2|\boldsymbol{J}|\,\mathrm{d}\xi\mathrm{d}\eta \tag{2}$$

where w is the transverse displacement and the over dot on it is the first order derivative with respect to time t; S the tension per unit length; ρ the mass per unit area; A the area of the membrane element; and $|\boldsymbol{J}|$ the determinant of Jacobian matrix. ξ and η are coordinates in the regular domain.

1.2 Sub-parametric quadrature membrane element

To develop a sub-parametric quadrature membrane element, the arbitrary shaped membrane element is firstly mapped into a regular domain shown in Fig.1, and then displacement is assumed as the function of ξ and η ($-1\leqslant\xi,\eta\leqslant1$). To increase the mapping accuracy, blending functions are used, namely [3,6,16]

$$\begin{cases}x=\dfrac{(1+\eta)}{2}X_3(\xi)+\dfrac{(1-\eta)}{2}X_1(\xi)+\dfrac{(1+\xi)}{2}X_2(\eta)+\dfrac{(1-\xi)}{2}X_4(\eta)-\dfrac{(1+\xi)(1+\eta)}{4}X_2(1)-\\ \qquad\dfrac{(1+\xi)(1-\eta)}{4}X_1(1)-\dfrac{(1-\xi)(1+\eta)}{4}X_3(-1)-\dfrac{(1-\xi)(1-\eta)}{4}X_4(-1)\\ y=\dfrac{(1+\eta)}{2}Y_3(\xi)+\dfrac{(1-\eta)}{2}Y_1(\xi)+\dfrac{(1+\xi)}{2}Y_2(\eta)+\dfrac{(1-\xi)}{2}Y_4(\eta)-\dfrac{(1+\xi)(1+\eta)}{4}Y_2(1)-\\ \qquad\dfrac{(1+\xi)(1-\eta)}{4}Y_1(1)-\dfrac{(1-\xi)(1+\eta)}{4}Y_3(-1)-\dfrac{(1-\xi)(1-\eta)}{4}Y_4(-1)\end{cases} \tag{3}$$

where $X_i(s)$ and $Y_i(s)(i=1,2,3,4;s=\xi\text{ or }\eta)$ are the parametric equations of the four edges of the membrane element.

To calculate the first order derivatives with respect to x and y, the chain rule of the partial differentiation is used

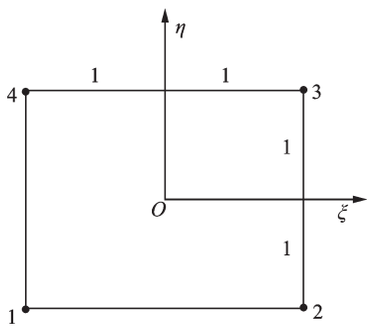

Fig.1 Sketch of a regular domain

$$\begin{Bmatrix} \frac{\partial w}{\partial x} \\ \frac{\partial w}{\partial y} \end{Bmatrix} = \begin{bmatrix} \frac{\partial \xi}{\partial x} & \frac{\partial \eta}{\partial x} \\ \frac{\partial \xi}{\partial y} & \frac{\partial \eta}{\partial y} \end{bmatrix} \begin{Bmatrix} \frac{\partial w}{\partial \xi} \\ \frac{\partial w}{\partial \eta} \end{Bmatrix} = \begin{bmatrix} \xi_x & \eta_x \\ \xi_y & \eta_y \end{bmatrix} \begin{Bmatrix} \frac{\partial w}{\partial \xi} \\ \frac{\partial w}{\partial \eta} \end{Bmatrix} = \boldsymbol{J}^{-1} \begin{Bmatrix} \frac{\partial w}{\partial \xi} \\ \frac{\partial w}{\partial \eta} \end{Bmatrix} \tag{4}$$

where $\boldsymbol{J}^{-1}$ is the inverse of Jacobian matrix.

Jacobian matrix $\boldsymbol{J}$ can be easily computed by Eq.(3) as

$$\boldsymbol{J} = \begin{bmatrix} \frac{\partial x}{\partial \xi} & \frac{\partial y}{\partial \xi} \\ \frac{\partial x}{\partial \eta} & \frac{\partial y}{\partial \eta} \end{bmatrix} = \begin{bmatrix} x_\xi & y_\xi \\ x_\eta & y_\eta \end{bmatrix} \tag{5}$$

The inverse of Jacobian matrix $\boldsymbol{J}^{-1}$ is given by

$$\boldsymbol{J}^{-1} = \frac{1}{(x_\xi y_\eta - x_\eta y_\xi)} \begin{bmatrix} y_\eta & -y_\xi \\ -x_\eta & x_\xi \end{bmatrix} = \frac{1}{|\boldsymbol{J}|} \begin{bmatrix} y_\eta & -y_\xi \\ -x_\eta & x_\xi \end{bmatrix} \tag{6}$$

Substituting Eq.(6) into Eq.(4) gives

$$\begin{cases} \frac{\partial w}{\partial x} = \frac{y_\eta}{|\boldsymbol{J}|} \frac{\partial w}{\partial \xi} - \frac{y_\xi}{|\boldsymbol{J}|} \frac{\partial w}{\partial \eta} \\ \frac{\partial w}{\partial y} = \frac{x_\xi}{|\boldsymbol{J}|} \frac{\partial w}{\partial \eta} - \frac{x_\eta}{|\boldsymbol{J}|} \frac{\partial w}{\partial \xi} \end{cases} \tag{7}$$

It is worth noting that $\partial w/\partial x$ and $\partial w/\partial y$ do not exist numerically at a point (ξ_i, η_i) if $\left|J(\xi_i, \eta_i)\right| = 0$.

Let N be the number of nodes in either ξ or η direction and $(\xi_j, \eta_i)(i, j = 1, 2, \cdots, N)$ be the coordinates of element nodes. The element displacement is assumed as

$$w(\xi, \eta, t) = \sum_{i=1}^{N} \sum_{j=1}^{N} l_j(\xi) l_i(\eta) w(\xi_j, \eta_i, t) = \sum_{i=1}^{N} \sum_{j=1}^{N} l_j(\xi) l_i(\eta) w_{ij}(t) \tag{8}$$

where $l_j(\xi)$ and $l_i(\eta)$ are shape functions.

It is reported that p-FEM with trigonometric functions are numerically more stable than orthogonal polynomials as the order is increased[3]. Since both the QEM and the p-FEM are weak form methods, therefore, trigonometric functions are used as the shape functions of the QEM, shown as

$$\begin{cases} l_j(\xi) = \prod_{\substack{k=1 \\ k \neq j}}^{N} \frac{\sin(p[\xi - \xi_k])}{\sin(p[\xi_j - \xi_k])} \\ l_i(\eta) = \prod_{\substack{k=1 \\ k \neq i}}^{N} \frac{\sin(p[\eta - \eta_k])}{\sin(p[\eta_i - \eta_k])} \\ i, j = 1, 2, \cdots, N; \xi, \eta \in [-1, 1] \end{cases} \tag{9}$$

where p ($\leqslant \pi/4$) is a control variable. When p is very small, Eq.(9) is equivalent to the polynomial-based shape functions.

The shape functions are new and used to develop a quadrature element for the first time, although Eq.(9) is widely used to compute the weighting coefficients in the strong form harmonic differential quadrature (HDQ) method[20].

Substituting Eq.(8) into Eq.(1) and performing the numerical integration by Gauss quadrature yield that

$$U = \frac{S}{2} \sum_{i=1}^{M} \sum_{j=1}^{M} H_i H_j B(\bar{\xi}_j, \bar{\eta}_i)^{\mathrm{T}} B(\bar{\xi}_j, \bar{\eta}_i) \left| J(\bar{\xi}_j, \bar{\eta}_i) \right| = \frac{1}{2} \boldsymbol{w}^{\mathrm{T}} \boldsymbol{k} \boldsymbol{w} \qquad N \leqslant M \tag{10}$$

where $\bar{\xi}_j, \bar{\eta}_i (i, j = 1, 2, \cdots, M)$ are the abscissas of Gauss quadrature and H_i, H_j the corresponding weights; $\boldsymbol{k}$ is the stiffness matrix and $\boldsymbol{w}$ the nodal displacement vector; $B(\bar{\xi}_j, \bar{\eta}_i)$ is

$$B(\bar{\xi}_j, \bar{\eta}_i) = \begin{bmatrix} \frac{y_\eta}{\left| J(\bar{\xi}_j, \bar{\eta}_i) \right|} \sum_{l=1}^{N} \sum_{k=1}^{N} A_{jk}^{\xi} l_l(\bar{\eta}_i) w_{lk} - \frac{y_\xi}{\left| J(\bar{\xi}_j, \bar{\eta}_i) \right|} \sum_{l=1}^{N} \sum_{k=1}^{N} l_k(\bar{\xi}_j) A_{il}^{\eta} w_{lk} \\ \frac{x_\xi}{\left| J(\bar{\xi}_j, \bar{\eta}_i) \right|} \sum_{l=1}^{N} \sum_{k=1}^{N} l_k(\bar{\xi}_j) A_{il}^{\eta} w_{lk} - \frac{x_\eta}{\left| J(\bar{\xi}_j, \bar{\eta}_i) \right|} \sum_{l=1}^{N} \sum_{k=1}^{N} A_{jk}^{\xi} l_l(\bar{\eta}_i) w_{lk} \end{bmatrix} \quad i, j = 1, 2, \cdots, M \tag{11}$$

where superscripts ξ or η mean that the corresponding first order derivative is taken with respect to ξ or η. More precisely, A_{jk}^{ξ} and A_{il}^{η} are the weighting coefficients of the first order derivative with respect to ξ and η.

The weighting coefficients A_{jk}^{ξ} can be explicitly calculated by

$$A_{jk}^{\xi}=\frac{\partial l_k(\bar{\xi}_j)}{\partial \xi}=\sum_{\substack{n=1\\ n\neq k}}^{N}\left[p\prod_{\substack{m=1\\ m\neq k,n}}^{N}\cos(p[\bar{\xi}_l-\xi_n])\sin(p[\bar{\xi}_l-\xi_m])\Big/\prod_{\substack{m=1\\ m\neq k}}^{N}\sin(p[\xi_k-\xi_m])\right]\quad j=1,2,\cdots,M \tag{12}$$

A_{il}^{η} can be calculated in a similar way. In this way, $\boldsymbol{k}$ can be obtained explicitly for any N and nodes of any type.

It is worth noting that Eq.(12) is reduced to the formulas of the weighting coefficient in the HDQ method[20] if the integration points are also the nodes. If $l_j(\xi)$ and $l_i(\eta)$ are Lagrange interpolation functions with polynomials which are commonly used in the QEM, a similar formula to Eq.(12) is also available to compute the weighting coefficient A_{jk}^{ξ}[17-18].

Substituting Eq.(8) into Eq.(2) and performing the numerical integration by Gauss quadrature yield that

$$T=\frac{\rho}{2}\sum_{i=1}^{M}\sum_{j=1}^{M}H_iH_jL(\bar{\xi}_j,\bar{\eta}_i)L(\bar{\xi}_j,\bar{\eta}_i)\left|\boldsymbol{J}(\bar{\xi}_j,\bar{\eta}_i)\right|=\frac{1}{2}\dot{\boldsymbol{w}}^{\mathrm{T}}\boldsymbol{m}\dot{\boldsymbol{w}}\quad N\leqslant M \tag{13}$$

where $\boldsymbol{m}$ is the mass matrix and $\dot{\boldsymbol{w}}$ the nodal velocity vector. $L(\bar{\xi}_j,\bar{\eta}_i)$ is shown as

$$L(\bar{\xi}_j,\bar{\eta}_i)=\sum_{l=1}^{N}\sum_{k=1}^{N}l_k(\bar{\xi}_j)l_l(\bar{\eta}_i)w_{lk}\qquad i,j=1,2,\cdots,M \tag{14}$$

It is seen that neither the type of nodes nor the number of nodes is fixed a priori in the derivations of the explicit formulas. Therefore, different types of nodes can be used and the solution accuracy can be easily adjusted by changing the number of the nodes in the developed program.

For free vibration analysis, $w(\xi,\eta,t)=W(\xi,\eta)\sin\omega t$ and thus $\boldsymbol{w}=\boldsymbol{W}\sin\omega t$, where ω is the circular frequency. After dropping the term $\sin\omega t$, the equation of motion is given by

$$\boldsymbol{kW}=\omega^2\boldsymbol{mW} \tag{15}$$

If more elements are used, the assemblage procedures are similar to the conventional finite element method (FEM). After applying the essential boundary condition, the matrix equation is modified as

$$\tilde{\boldsymbol{k}}\tilde{\boldsymbol{W}}=\omega^2\tilde{\boldsymbol{m}}\tilde{\boldsymbol{W}} \tag{16}$$

Solving Eq.(16) by a generalized eigen-value solver yields the frequencies and mode shapes.

2 Numerical Results and Discussion

For demonstrations, the widely used Gauss-Lobatto-Legendre (GLL) points in QEM are adopted as the element nodes. An explicit formula to calculate the GLL points does not exist and thus the program reported in Ref.[12] is used to compute $\xi_k,\eta_k(k=1,2,\cdots,N)$. Mapping an irregular domain without four corners into a regular one is more difficult than the one with four corners, since $|\boldsymbol{J}|=0$ at the added corner point[16]. Therefore, examples of irregular shaped membranes with a part of an elliptic shape (Fig.2(a)), full elliptic shape (Fig.2(b)), half circle+triangle (Fig.3), and general quadrilateral shape, are given. In Figs.2, 3, symbols ① — ④ represent the four edges of the membrane element which are needed in Eq.(3). Besides, only one $N\times N$-node element with $p=\pi/8$ is used in the analysis, since $p=\pi/8$ is widely used in the HDQ method and different values of p affect only the higher mode frequencies which are not studied in this paper. All edges of the membranes are fixed, i.e., $w=0$ on all edges.

The non-dimensional frequency parameter Ω is defined as

$$\Omega=\omega a\sqrt{\rho/S} \tag{17}$$

where a is the semi-major axis of the ellipse (Fig.2) or the radius of the circle (Fig.3).

Example 1 First, consider the free vibration of a sectorial membrane shown in Fig.2(a). To map

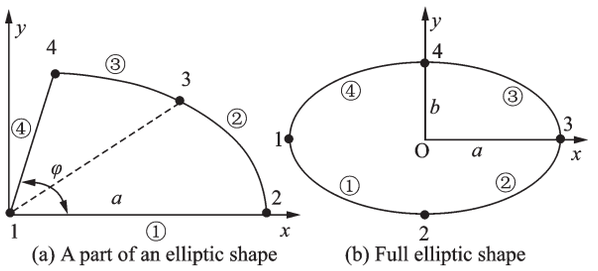

Fig.2 Sketches of arbitrary shaped membranes

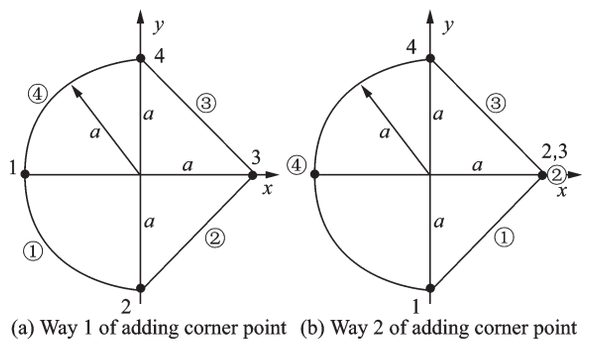

Fig.3 Sketche of a half-circle+triangle membrane

it into a regular domain with four corners, as shown in Fig.1, one additional corner point is needed. Currently the point, i.e., point 3 shown in Fig.2(a), is located on the curved edge. Other ways to set the additional corner point exist and the effect on the final results is negligible if the mapping is accurate enough[16].

The parametric equations of the four edges of the sectorial membrane, as shown in Fig.2(a), are

$$\begin{cases} X_1(\xi)=0.5(1+\xi)a \\ Y_1(\xi)=0 \\ X_2(\eta)=a\cos[(1+\eta)\theta/4] \\ Y_2(\eta)=b\sin[(1+\eta)\theta/4] \\ X_3(\xi)=a\cos[(3-\xi)\theta/4] \\ Y_3(\xi)=b\sin[(3-\xi)\theta/4] \\ X_4(\eta)=0.5(1+\eta)a\cos\theta \\ Y_4(\eta)=0.5(1+\eta)b\sin\theta \end{cases} \tag{18}$$

where θ equals to $\mathrm{arctg}(a*\tan(\varphi)/b)$; a and b are the semi-major and semi-minor axes of the elliptic curve.

The first 10 non-dimensional frequencies are listed in Table 1. The number of nodes in each direction varies from 7 to 12. Available exact solutions and data obtained by conventional and p-version finite element methods, denoted by c-FEM and p-FEM, are included for comparisons.

Table 1 Comparison of non-dimensional frequency parameter Ω for sectorial membrane ($\varphi=\pi/2$)

Condition	1	2	3	4	5	6	7	8	9	10
QEM(N=7)	5.137	7.589	8.420	9.934	11.071	11.630	12.358	14.066	15.393	15.590
QEM(N=9)	5.136	7.588	8.417	9.936	11.065	11.620	12.230	13.617	14.419	14.506
QEM(N=11)	5.136	7.588	8.417	9.936	11.065	11.620	12.225	13.590	14.373	14.476
QEM(N=12)	5.136	7.588	8.417	9.936	11.065	11.620	12.225	13.589	14.373	14.476
c-FEM	5.136	7.589	8.417	9.937	11.065	11.621	12.226	13.590	14.374	14.477
p-FEM(p=12)[3]	5.136	7.589	8.417	9.937	11.065	11.620	12.228	13.591	14.373	14.482
Exact[3]	5.136	7.588	8.417	9.936	11.065	11.620	12.225	13.589	14.373	14.476

It is seen that the present element is highly accurate. Exact first three non-dimensional frequency parameters can be obtained by using one 9×9-node element. When N is 12, all 10 non-dimensional frequency parameters are numerically exact. The conventional FEM with fine meshes and the p-version FEM using trigonometric sine functions with p=12 yield slightly lower accurate solutions for higher modes.

The first eight non-dimensional frequencies for sectorial membranes with different sector angles and aspect ratios are listed in Table 2. To ensure the solution accuracy, one 14×14-node element is used. Obtained results agree well with the data using the

conventional finite element with fine meshes. The QEM results listed in Table 2 should be highly accurate according to the observation from Table 1 and thus can serve as references.

Example 2 Second, consider the free vibration of an elliptic membrane shown in Fig.2(b). To map it into a regular domain with four corners, as shown in Fig.1, four corner points are needed. Currently four corner points on the curved edge shown in Fig.2(b) are adopted. Other ways to set the four corner points are available and the final results are independent from the way to place the corner points[16].

The parametric equations of the four edges of the elliptic membrane shown in Fig.2(b) are

$$\begin{cases} X_1(\xi) = -a\cos[(1+\xi)\pi/4] \\ Y_1(\xi) = -b\sin[(1+\xi)\pi/4] \\ X_2(\eta) = a\cos[(1-\eta)\pi/4] \\ Y_2(\eta) = -b\sin[(1-\eta)\pi/4] \\ X_3(\xi) = a\cos[(1-\xi)\pi/4] \\ Y_3(\xi) = b\sin[(1-\xi)\pi/4] \\ X_4(\eta) = -a\cos[(1+\eta)\pi/4] \\ Y_4(\eta) = b\sin[(1+\eta)\pi/4] \end{cases} \tag{19}$$

where a and b are the semi-major and semi-minor axes of the elliptic membrane.

The first ten non-dimensional frequencies are listed in Table 3. The number of nodes in each direction varies from 7 to 14. Available exact solutions and data obtained by DQEM are included for comparisons.

Table 2 Non-dimensional frequency parameter Ω for various sectorial membranes ($N=14$)

Condition		1	2	3	4	5	6	7	8
$\varphi=\pi/2$	QEM	7.981	10.408	12.991	14.199	15.671	16.477	18.412	18.473
$a/b=2$	c-FEM	7.981	10.408	12.992	14.200	15.672	16.478	18.413	18.874
$\varphi=\pi/2$	QEM	11.039	13.323	15.755	18.303	20.420	20.941	22.586	23.647
$a/b=3$	c-FEM	11.040	13.324	15.755	18.304	20.426	20.944	22.592	23.653
$\varphi=\pi/3$	QEM	6.380	9.761	9.936	13.015	13.354	13.589	16.223	16.698
$a/b=1$	c-FEM	6.380	9.761	9.936	13.015	13.354	13.590	16.225	16.700
$\varphi=\pi/3$	QEM	8.698	11.631	14.435	15.419	17.294	18.542	20.024	21.417
$a/b=2$	c-FEM	8.698	11.630	14.436	15.420	17.295	18.544	20.027	21.422
$\varphi=\pi/3$	QEM	11.564	14.197	16.936	19.692	21.209	22.564	23.885	25.381
$a/b=3$	c-FEM	11.565	14.198	16.938	19.695	21.213	22.570	23.890	25.379

Table 3 Comparison of non-dimensional frequency parameter Ω for a circular membrane

Condition	1	2	3	4	5	6	7	8	9	10
QEM(N=7)	2.404 8	3.836 5	3.836 5	5.122 3	5.172 3	5.505 9	6.510 7	6.510 7	7.757 8	7.966 0
QEM(N=9)	2.404 8	3.831 8	3.831 8	5.133 8	5.136 6	5.517 5	6.393 6	6.393 6	7.094 3	7.094 3
QEM(N=11)	2.404 8	3.831 7	3.831 7	5.135 6	5.135 6	5.520 0	6.380 8	6.380 8	7.020 0	7.020 0
QEM(N=13)	2.404 8	3.831 7	3.831 7	5.135 6	5.135 6	5.520 1	6.380 2	6.380 2	7.015 7	7.015 7
QEM(N=14)	2.404 8	3.831 7	3.831 7	5.135 6	5.135 6	5.520 1	6.380 2	6.380 2	7.015 6	7.015 6
DQEM[5]	2.403 0	3.828 8	3.828 8	5.126 9	5.126 9	5.515 9	6.375 3	6.375 3	7.010 3	7.010 3
DQEM[6]	2.404 8	3.831 7	3.831 7	5.135 6	5.135 6	5.520 1	6.380 2	6.380 2	7.015 6	7.015 6
c-FEM[2]	2.416 6	3.851 3	3.851 3	5.174 4	5.174 4	5.551 5	6.461 0	6.461 0	7.059 2	7.059 2
c-FEM	2.404 8	3.831 8	3.831 8	5.135 7	5.135 7	5.520 2	6.380 2	6.380 2	7.015 7	7.015 7
Exact[5]	2.404 8	3.831 7	3.831 7	5.135 6	5.135 6	5.520 1	6.380 2	6.380 2	7.015 6	7.015 6

It is seen that the present element is highly accurate. one 14×14-node element (196 DOFs) can yield ten numerically exact frequencies. Numerically exact first ten frequencies are also obtained by the DQEM[6] employing the same geometric mapping with 17×17 grid points (289 DOFs). Perhaps due to inaccurate mapping, the DQEM[5] can only yield approximate solutions even with 41×41 grid points (1 681 DOFs). It is expected that the solutions obtained by lower order finite element (1 024 DOFs)[2] are not accurate enough. If a very fine mesh is used, the accuracy of the recalculated data by the lower order finite element can be improved greatly. The smallest number of DOFs demonstrates the effectiveness of the QEM.

The first eight non-dimensional frequencies for elliptic membranes with different aspect ratios are listed in Table 4. To ensure the solution accuracy, one 14×14-node element is used. Obtained results agree well with the DQEM (17×17) data using the same geometric mapping technique. The results listed in Table 4 should be highly accurate and thus can serve as references.

Table 4 Non-dimensional frequency parameter Ω for various elliptic membranes ($N=14$)

Condition		1	2	3	4	5	6	7	8
$\frac{a}{b}=1.5$	QEM	3.058 7	4.373 4	5.317 3	5.761 5	6.506 7	7.183 9	7.654 2	7.754 7
	DQEM[6]	3.058 7	4.373 4	5.317 3	5.761 5	6.506 7	7.183 9	7.654 2	7.754 7
$\frac{a}{b}=2.0$	QEM	3.777 2	5.010 2	6.333 5	6.851 8	7.714 2	7.981 0	9.131 7	9.170 2
	DQEM[6]	3.777 2	5.010 2	6.333 5	6.851 8	7.714 2	7.981 0	9.131 7	9.170 2
$\frac{a}{b}=2.5$	QEM	4.525 7	5.704 0	6.970 8	8.301 5	8.403 9	9.499 6	9.678 1	10.648
	DQEM[6]	4.525 7	5.704 0	6.970 8	8.301 5	8.403 9	9.499 6	9.678 1	10.648
$\frac{a}{b}=3.0$	QEM	5.289 0	6.430 8	7.654 0	8.940 8	9.963 7	10.277	11.039	11.652
	DQEM[6]	5.289 0	6.430 8	7.654 0	8.940 8	9.963 7	10.277	11.039	11.651

The accuracy of geometric mapping affects the solution accuracy greatly[6,15]. To demonstrate it, shape functions of G-node serendipity element $f_i(\xi,\eta)$ are used for geometric mapping

$$\begin{cases} x=x(\xi,\eta)=\sum_{i=1}^{G}f_i(\xi,\eta)x_i \\ y=y(\xi,\eta)=\sum_{i=1}^{G}f_i(\xi,\eta)y_i \end{cases} \quad -1\leqslant\xi,\eta\leqslant1 \tag{20}$$

The percentage relative error listed in Table 5 is defined as $\mathrm{Err}=(A-\pi ab)/(\pi ab)*100\%$, where A is the mapped area. The general shape functions of the 12-node serendipity element with non-uniformly distributed nodes are given in Ref.[16].

The fundamental frequencies of various elliptic membranes are listed in Table 5. Geometric mapping is performed using Eq.(20) ($G=8$ or 12). Available data obtained by the DSC with $N=15$[4] and the DQEM with $N=41$[5] are included for comparisons.

It is seen that both the weak form QEM and the strong form DQEM yield the same convergent results if the same mapping technique is used. The mapping error obviously affects the solution accuracy obtained by various numerical methods. Employing non-uniformly distributed nodes such as the GLL nodes does improve the mapping accuracy and thus improves the accuracy of solutions. Therefore, accurate mapping technique should be always used to obtain highly accurate results.

Example 3 Further consider the free vibration of a half-circle+triangle membrane shown in Fig.3. To map it into a regular domain with four corners shown in Fig.1, one more corner point is needed. Two ways of adding the corner point are shown in Fig.3. If the curved edge becomes straight, it reduces to a triangular element.

The parametric equations of the four edges of

Table 5 Effect of the mapping accuracy on the fundamental frequency of various elliptic membranes

$\frac{a}{b}$	Exact	8-node serendipity element			12-node serendipity element		
		Uniformly distributed nodes			Uniformly distributed nodes		GLL nodes
		QEM(N=11)	DSC[4]	DQEM[5]	QEM(N=11)	DQEM[5]	QEM(N=11)
1.0	2.404 8	2.419 4	2.406	2.419 4	2.403 0	2.403 0	2.405 1
1.5	3.058 7	3.077 7	3.062	3.077 7	3.056 0	3.061 9	3.058 6
2.0	3.777 2	3.801 8	3.784	3.801 7	3.773 2	3.773 3	3.776 2
2.5	4.525 7	4.556 5	4.535	4.556 4	4.520 2	4.520 3	4.523 5
3.0	5.289 0	5.326 3	—	5.326 2	5.281 7	5.281 8	5.285 4
Err/%		−1.178 5			0.157 45		−0.018 73

the irregular shaped membrane shown in Fig. 3(a) and Fig.3(b) are

$$\begin{cases} X_1(\xi)=-a\cos[(1+\xi)\pi/4] \\ Y_1(\xi)=-a\sin[(1+\xi)\pi/4] \\ X_2(\eta)=a(1+\eta)/2] \\ Y_2(\eta)=-a(1-\eta)/2] \\ X_3(\eta)=a(1+\xi)/2] \\ Y_3(\eta)=a(1-\xi)/2] \\ X_4(\eta)=-a\cos[(1+\eta)\pi/4] \\ Y_4(\eta)=a\sin[(1+\eta)\pi/4] \end{cases} \tag{21}$$

$$\begin{cases} X_1(\xi)=a(1+\xi)/2] \\ Y_1(\xi)=-a(1-\xi)/2] \\ X_2(\eta)=a \\ Y_2(\eta)=0 \\ X_3(\xi)=a(1+\xi)/2] \\ Y_3(\xi)=a(1-\xi)/2] \\ X_4(\eta)=-a\cos(\eta\pi/2) \\ Y_4(\eta)=a\sin(\eta\pi/2) \end{cases} \tag{22}$$

where a is the radius of the half circle.

The first eight non-dimensional frequencies obtained using Eq.(21) are listed in Table 6. The number of nodes in each direction varies from 7 to 14. Existing solutions obtained by other numerical methods are included for comparisons. Results with Eq.(22) are similar to the ones with Eq.(21) and thus only the ones with N=14 are included for comparisons.

Since exact solutions are not available, the highly accurate DQEM data cited from Ref. [6] (289 DOFs) are used for comparisons. It is seen that accurate non-dimensional frequency parameters can be obtained by using one 13×13-node (169 DOFs) element with Eq.(21). The accuracy of the QEM with Eq.(22) is slightly lower. Due to the mapping error, data obtained by the DQEM with N=41 (1 681 DOFs)[5] are still not accurate enough. Some frequencies obtained by the LRBFDQ with 1 675 DOFs[7] are not accurate enough. The data obtained by the lower order FEM with 1 089 DOFs[2] are obviously inaccurate. The accuracy of the FEM data with a fine mesh (5 221 DOFs) is much improved. Based on the total number of DOFs, one may conclude that the QEM is efficient and suitable for analysis of arbitrarily shaped membranes. Perhaps due to the fact of that the curved edge is much longer than the other two edges, the solution accuracy of the QEM with Eq.(22) is slightly lower than the one with Eq.(21) when N is small. The two ways to map the irregular shape without four corners into a regular one demonstrate the flexibility of the sub-parametric element formulations.

Example 4 Last, consider the free vibration of a general quadrilateral membrane. The Cartesian coordinates of four corners are (0.0, 0.0), (3.0, 0.0), (2.5, 2.5) and (0.5, 2.0) for comparing with existing data.

The irregular domain can be exactly mapped in-

Table 6 Comparison of non-dimensional frequency parameter Ω for the half-circle+triangle membrane

Condition	1	2	3	4	5	6	7	8
QEM-a(N=7)	2.710 7	4.233 7	4.359 2	5.583 7	5.924 4	6.110 0	7.012 2	7.304 3
QEM-a(N=9)	2.710 6	4.232 0	4.357 9	5.573 0	5.933 0	6.117 2	7.012 0	7.196 3
QEM-a(N=11)	2.710 6	4.231 9	4.357 9	5.572 7	5.933 9	6.117 9	7.013 1	7.188 1
QEM-a(N=13)	2.710 6	4.231 9	4.357 9	5.572 7	5.933 9	6.117 9	7.013 1	7.187 9
QEM-a(N=14)	2.710 6	4.231 9	4.357 9	5.572 7	5.933 9	6.117 9	7.013 1	7.187 9
QEM-b(N=14)	2.710 6	4.231 9	4.357 9	5.572 8	5.933 9	6.118 0	7.013 2	7.188 0
DQEM(N=41)[5]	2.710 6	4.232 1	4.357 8	5.568 9	5.937 3	6.118 2	7.007 3	7.186 8
DQEM(N=17)[6]	2.710 6	4.231 9	4.357 9	5.572 7	5.933 9	6.117 9	7.013 1	7.187 9
LRBFDQ (1675 DOFs)[7]	2.710 6	4.231 0	4.357 9	5.572 8	5.933 9	6.118 0	7.013 4	7.188 0
c-FEM (1089 DOFs)[2]	2.723 0	4.259 8	4.378 6	5.633 6	5.984 6	6.164 1	7.133 4	7.300 2
c-FEM (5221 DOFs)	2.710 9	4.232 9	4.358 9	5.574 7	5.936 8	6.120 9	7.017 2	7.192 5

to a regular one by Eq.(20) with G=4, where the shape functions are $f_i(\xi,\eta)=(1+\xi_i\xi)(1+\eta_i\eta)/4$ (i=1, 2, 3, 4). For comparisons with the existing data, a slightly different frequency parameter Ω^* from Eq.(17) is used, shown as

$$\Omega^* = \omega\sqrt{\rho/S} \tag{23}$$

The first eight frequencies parameters are listed in Table 7. The results are exactly the same as the DQEM ones. Since the geometric mapping is exact, the data in Ref.[5] should be very accurate. As expected, the conventional FEM can also yield accurate results since all edges are straight.

Table 7 Comparison of the frequency parameter Ω^* for the general quadrilateral membrane

Condition	1	2	3	4	5	6	7	8
QEM-a(N=7)	1.897 3	2.884 0	3.082 8	3.801 1	4.008 9	4.355 9	4.743 8	4.996 4
QEM-a(N=9)	1.897 3	2.883 8	3.082 5	3.800 6	4.008 6	4.357 3	4.737 8	4.990 4
QEM-a(N=11)	1.897 3	2.883 8	3.082 5	3.800 6	4.008 7	4.357 4	4.737 6	4.990 4
QEM-a(N=13)	1.897 3	2.883 8	3.082 5	3.800 6	4.008 7	4.357 4	4.737 6	4.990 4
DQEM(N=41)[5]	1.897 3	2.883 8	3.082 5	3.800 6	4.008 7	4.357 4	4.737 6	4.990 4
c-FEM (1812 DOFs)[5]	1.89	2.88	3.08	3.79	3.99	4.35	—	—

3 Conclusions

Free vibration of arbitrarily shaped membranes is analyzed by using the weak form quadrature element method. A novel sub-parametric element is developed. The element domain is accurately mapped into a regular one using blending functions. Trigonometric functions are used as the elemental displacement for the first time. To ease the programming, explicit formulas of a varying number of nodes are given. For verifications, results are compared with exact solutions and data obtained by other numerical methods. The solution accuracy can be improved by increasing the number of nodes easily. It is shown that highly accurate frequencies can be obtained by the proposed element with a small number of nodes. Accurate mapping plays an important role for successfully using both strong and weak form methods.

References

[1] JENKINS C H M, KORDE U A. Membrane vibration experiments: An historical review and recent results [J]. Journal of Sound and Vibration, 2006, 295: 602-613.

[2] KANG S W, LEE J M, KANG Y J. Vibration analy-

sis of arbitrarily shaped membranes using non-dimensional dynamic influence function[J]. Journal of Sound and Vibration, 1999, 221: 117-132.

[3] HOUMAT A. Free vibration analysis of arbitrarily shaped membranes using the trigonometric p-version of the finite-element method[J]. Thin-Walled Structures, 2006, 44: 943-951.

[4] CIVALEK Ö, GURSES M. Free vibration of curvilinear membranes by eight-node discrete singular convolution[J]. International Journal of Science and Technology, 2008, 3(2): 165-171.

[5] FANTUZZI N, TORNABENE F, VIOLA E. Generalized differential quadrature finite element method for vibration analysis of arbitrarily shaped membranes [J]. International Journal of Mechanical Sciences, 2014,79: 216-251.

[6] FANTUZZI N, DELLA P G, TORNABENE F, et al. Strong formulation isogeometric analysis for the vibration of thin membranes of general shape[J]. International Journal of Mechanical Sciences, 2017, 120: 322-340.

[7] WU W X, SHU C, WANG C M. Vibration analysis of arbitrarily shaped membranes using local radial basis function-based differential quadrature method[J]. Journal of Sound and Vibration, 2007, 306: 252-270.

[8] LIU N, JEFFERS A E. A geometrically exact isogeometric Kirchhoff plate: Feature-preserving automatic meshing and C1 rational triangular Bézier spline discretizations[J]. International Journal for Numerical Methods in Engineering, 2018, 115: 395-409.

[9] ZHONG H, YUE Z G. Analysis of thin plates by the weak form quadrature element method[J]. Science China Physics, Mechanics & Astronomy, 2012, 55: 861-871.

[10] TORNABENE F, FANTUZZI N, UBERTINI F, et al. Strong formulation finite element method based on differential quadrature: A survey[J]. Applied Mechanics Reviews, 2015, 67(2): 020801.

[11] WANG X, YUAN Z, DENG J. A review on the discrete singular convolution algorithm and its applications in structural mechanics and engineering[J]. Archives of Computational Methods in Engineering, 2020, 27(5): 1633-1660.

[12] WANG X, YUAN Z, JIN C. Weak form quadrature element method and its applications in science and engineering: A state-of-the-art review[J]. Applied Mechanics Reviews, 2017,69(3): 030801.

[13] ABRATE S. Vibration of point supported triangular plates[J]. Computers and Structures, 1996, 58(2): 327-336.

[14] XING Y, LIU B. High-accuracy differential quadrature finite element method and its application to free vibrations of thin plate with curvilinear domain[J]. International Journal for Numerical Methods in Engineering, 2009, 80: 1718-1742.

[15] BERT C W, MALIK M. The differential quadrature method for irregular domains and application to plate vibration[J]. International Journal of Mechanical Sciences, 1996, 38: 589-606.

[16] CAI D, ZHOU G, WANG X. On mapping irregular plates without four corners into a regular domain[J]. Applied Mathematics Letters, 2021,117: 107082.

[17] DENG J, WANG X, YUAN Z, et al. An efficient technique for simultaneous local and overall buckling analysis of stiffened panels[J]. Advances in Engineering Software, 2019, 131: 36-47.

[18] WANG Xinwei, YUAN Zhangxian. An efficient method for local buckling analysis of stiffened panels [J].Transactions of Nanjing University of Aeronautics and Astronautics, 2019, 36(1): 20-28.

[19] WILLBERG C, DUCZEK S, VIVAR P J M, et al. Comparison of different higher order finite element schemes for the simulation of Lamb waves[J]. Computer Methods in Applied Mechanics and Engineering, 2012, 241: 246-261.

[20] HE B, WANG X. Error analysis in differential quadrature method[J]. Transactions of Nanjing University of Aeronautics & Astronautics, 1994, 11(2): 194-200.

Acknowledgements This paper is partially supported by the National Natural Science Foundation of China (Nos. 52005256, 12072154), the Natural Science Foundation of Jiangsu Province (No.BK20190394), the Jiangsu Post-Doctoral Research Funding Program (No.2020Z437) and the Priority Academic Program Development of Jiangsu Higher Education Institutions. The present investigators are grateful for helpful discussions with Prof. **YUAN Zhangxian** of Worcester Polytechnic Institute, USA.

Author Prof. **WANG Xinwei** graduated in airplane design from Nanjing Aeronautical Institute, China, in 1975, and received his M.S. degree in solid mechanics from the same institute, in 1981 and Ph.D. degree in solid mechanics from School of Aerospace and Mechanical Engineering, University of Oklahoma, USA, in 1989. He was a professor in struc-

tural mechanics at the State Key Laboratory of Mechanics and Control of Mechanical Structures, Nanjing University of Aeronautics and Astronautics, China. His research interests include finite element method and its applications, efficient computational methods and their applications, and mechanical behavior of composite materials.

Author contributions Prof. **WANG Xinwei** designed the study and wrote the manuscript. Dr. **CAI Deng'an** conducted the analysis and interpreted the results. Prof. **ZHOU Guangming** contributed to the discussion and background of the study. All authors commented on the manuscript draft and approved the submission.

Competing interests The authors declare no competing interests.

(Production Editor: ZHANG Bei)

任意形状膜的求积单元振动分析

王鑫伟,蔡登安,周光明

(南京航空航天大学机械结构力学及控制国家重点实验室, 南京 210016, 中国)

摘要:本文目的是建立一种能够高效分析任意形状膜的自由振动的弱式求积单元。先采用融合函数将任意形状变换成规则的区域,然后将单元内的位移场假设为三角函数,最终导出了节点数目可变和节点类型任意的单元的显式表达式。为了验证本文方法的有效性,将得到的结果与精确解和采用其他数值方法的结果进行了对比。研究表明:本文方法可以用很少的节点数目给出高精度自由振动频率。

关键词:任意形状膜;自由振动;求积单元;融合函数